

# Space–Time Variations in the Attenuation Field of Short Period Shear Waves in the Hindu Kush Area

Yu. F. Kopnichev<sup>a, \*</sup> and I. N. Sokolova<sup>b, \*\*</sup>

<sup>a</sup>*Institute of Physics of the Earth, Russian Academy of Sciences, ul. B. Gruzinskaya 10, Moscow, 125395 Russia*

<sup>b</sup>*Institute of Geophysical Research, Ministry of Energy, Republic of Kazakhstan, ul. Chaikinoi 4, Alma-Ata, 050020 Russia*

\**e-mail: yufk777@mail.ru*

\*\**e-mail: sokolova@kndc.kz*

Received May 7, 2016

**Abstract**—This paper is concerned with space–time variations in the attenuation of shear waves in the Hindu Kush area. We examined the ratios of maximum amplitudes in S and P waves (the S/P parameter) obtained from records of deep-focus earthquakes made at the AAK station in 1993–2016 at epicentral distances of ~700–800 km. The dependence of the amplitude on the radiation pattern for S and P waves was taken into account by averaging the S/P parameter over different time spans. Substantial space–time variations in S wave attenuation was found in different depth ranges in the zone of deep-focus seismicity. We show that the lowest attenuation in 2013–2015 prior to the great earthquake of October 26, 2015 ( $M_w = 7.5$ ,  $h = 231$  km) was observed for hypocenters above the rupture zone, at depths of 151–210 km, while the highest attenuation occurred at depths of 231–270 km. Following the earthquake, the attenuation rapidly decreased at depths of 231–270 km and increased in the depth range of 191–230 km. These effects are hypothesized to have been caused by dehydration of mantle rocks, as well as by migration of deep-seated fluids.

DOI: 10.1134/S0742046318060040

## INTRODUCTION

The Hindu Kush zone of deep-focus seismicity has been studied in numerous publications (Roecker et al., 1980; Roecker, 1982; Pegler and Das, 1998, among others). Cross-sections of P and S velocity fields down to a depth of ~250 km have been constructed and the fields were shown to exhibit substantial inhomogeneities (Roecker, 1982). The spatial distribution of deep-focus earthquakes was studied (Roecker et al., 1980; Roecker, 1982; Pegler and Das, 1998), and relationships have been found to exist between great deep-focus and large crustal earthquakes in the extensive area of Central and South Asia (Kopnichev et al., 2002). At the same time, it has to be admitted that the issue of the origin for this zone of deep-focus seismicity is far from being resolved. More seismic and geophysical data should be acquired in order to answer this question. The present study approaches the issue by considering the attenuation of S waves in the zone of deep-focus seismicity and presents a comparison of these data with seismicity features. Special attention is focused on an analysis of space–time variations in the attenuation field in the rupture zone of a recent great earthquake (October 26, 2015,  $M_w = 7.5$ ) and its nearest environs.

## HISTORICAL SEISMICITY

The deep-focus seismicity beneath the Hindu Kush is concentrated in the depth range of ~70–300 km (Pegler and Das, 1998). Table 1 presents data on  $M \geq 7.0$  earthquakes that have occurred in the region since the beginning of the 20th century. This table shows that a total of 12 such earthquakes have occurred for the past 115 years. The occurrence of these earthquakes between 1965 and 2002 was periodic, with the period being approximately 9 years. From 2002 onward the periodicity broke down, with the next large  $M_w = 7.5$  earthquake occurring on October 26, 2015 (see Table 1).

Figure 1 shows the depth-dependent distribution of large deep-focus ( $h > 100$  km) earthquakes beneath the Hindu Kush since 1973, when depths began to be determined with lesser uncertainty. It follows from Fig. 1 and Table 1 that 11  $M \geq 6.5$  earthquakes have occurred at depths of 181–231 km, with the hypocenters of all five  $M \geq 7.0$  earthquakes falling in a relatively narrow range,  $h = 210$ –231 km. Interestingly, the epicenters of only 2 of the 11 earthquakes were west of 70.5°E, and both of these events occurred later than 2001 (Fig. 2). The epicenters of the other earthquakes were east of 70.7°E.

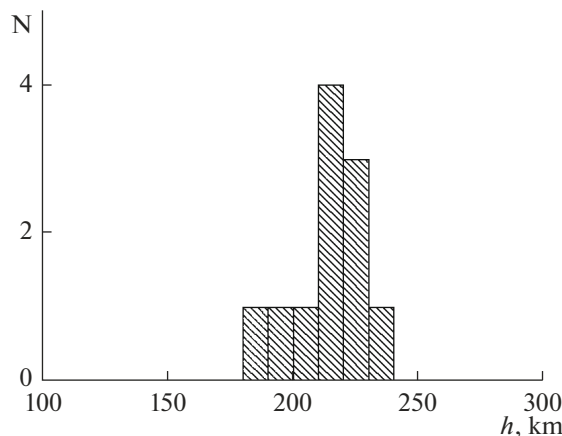
This distribution of the events over depth in an intracontinental region is substantially different from

**Table 1.** The parameters of  $M \geq 7.0$  earthquakes since 1900 beneath Hindu Kush

Date	°N	°E	$h$ , km	$M$
24 Oct 1908	36.5	70.5	220	7.0
7 Aug 1909	36.5	70.5	230	7.6
4 Jul 1911	36.0	70.5	190	7.4
15 Nov 1921	36.12	70.72	152	7.6
1 Feb 1929	36.46	70.93	208	7.0
4 Mar 1949	36.0	70.5	230	7.4
14 Mar 1965	36.40	70.71	210	7.5
30 Jul 1974	36.37	70.73	210	7.1
30 Dec 1983	36.39	70.71	215	7.4
29 Jul 1985	36.16	70.86	100	7.4
9 Aug 1993	36.33	70.87	211	7.0
3 Mar 2002	36.50	70.48	225	7.4
26 Oct 2015	36.53	70.36	231	7.5

that in various subduction zones, where both the seismicity rate and the total seismic energy commonly steadily decrease over depth down to  $h \sim 300$  km (Kalinin et al., 1989; Levin and Sasorova, 2012).

Figure 3 shows the 1-month aftershocks of the October 26, 2015 earthquake. The aftershocks make a compact area that is elongate nearly east–west and is  $\sim 30$  km across. The hypocenter depths vary in the range between 190 and 219 km, with most of the events (30 of 37) being at depths of 190–210 km. It is notable that the aftershock area is appreciably higher than the mainshock hypocenter. It should also be noted that anomalously numerous deep-focus  $M \geq 4.0$  events were recorded in the depth range of 150–270 km during 4 months after the October 26, 2015 earthquake ( $n = 78$  events, including “remote” aftershocks between  $70^\circ$  and  $72^\circ$  E). For comparison we may note

**Fig. 1.** A histogram showing the number of large ( $M \geq 6.5$ ) earthquakes in the Hindu Kush area plotted against depth.

that the large earthquakes of August 9, 1993 ( $M_w = 7.0$ ) and March 3, 2002 ( $M_w = 7.4$ ) were followed within 4 months by only 9 and 17 events of this size, respectively. This large number of aftershocks made it possible to examine the attenuation variation in the rupture zone and its near environs in detail after the Hindu Kush earthquake of October 26, 2015.

### THE OBSERVATION SYSTEM AND THE EXPERIMENTAL DATA

We analyzed records of Hindu Kush earthquakes in the depth range of 150–270 km made at the Ala–Archa station (AAK) in 1993–2016 (Fig. 4). The magnitudes were within the 4.0–6.0 range and the epicentral distances varied between 700 and 800 km. A total of over 800 records were used.

The studied depth range was subdivided into four layers: 151–190, 191–210, 211–230, and 231–270 km. We note that the hypocenters were distributed rather uniformly in the three upper layers, while in the bottom layer over 80% of all events occurred at depths of 231–250 km. Considering the location and dimensions of the aftershock area for the October 26, 2015 earthquake, we subdivided the volume of interest into three regions, one of which (the central one, between  $70.20^\circ$  and  $70.55^\circ$  E) is nearly identical with the aftershock area in map view. The other two regions ( $69.80^\circ$ – $70.20^\circ$  E and  $70.55^\circ$ – $71.30^\circ$  E) were west and east of the aftershock area, respectively.

### MATERIALS AND METHODS

Since  $Q$  is a function of frequency, we allowed for this by performing narrow-band filtering of the vertical-component records using a filter centered at 1.25 Hz, whose bandwidth was  $2/3$  octaves at 0.7 of the maximum (Kopnichev, 1985).

We measured the ratios between the peak amplitudes in P and S waves (the  $\log(AS/AP)$  parameter, which will be denoted as S/P for brevity). Obviously, an increase in S/P corresponds, all other things being equal, to a decrease in the effective attenuation of short-period shear waves, and vice versa (Kopnichev and Sokolova, 2007).

It should be noted that the S/P level is substantially affected by the radiation pattern for S and P waves, as well as by inhomogeneities in the attenuation field around the recording station (Kopnichev and Sokolova, 2007). The influence of the first of these factors was incorporated by averaging S/P in each depth range. More often, we averaged data over 1 or 2 years, and less often over longer time intervals, depending on the number of seismograms. We note that the averaging for 2015 was conducted separately for the period before October 26 (for foreshocks of that earthquake) and after October 26 (for the aftershocks).

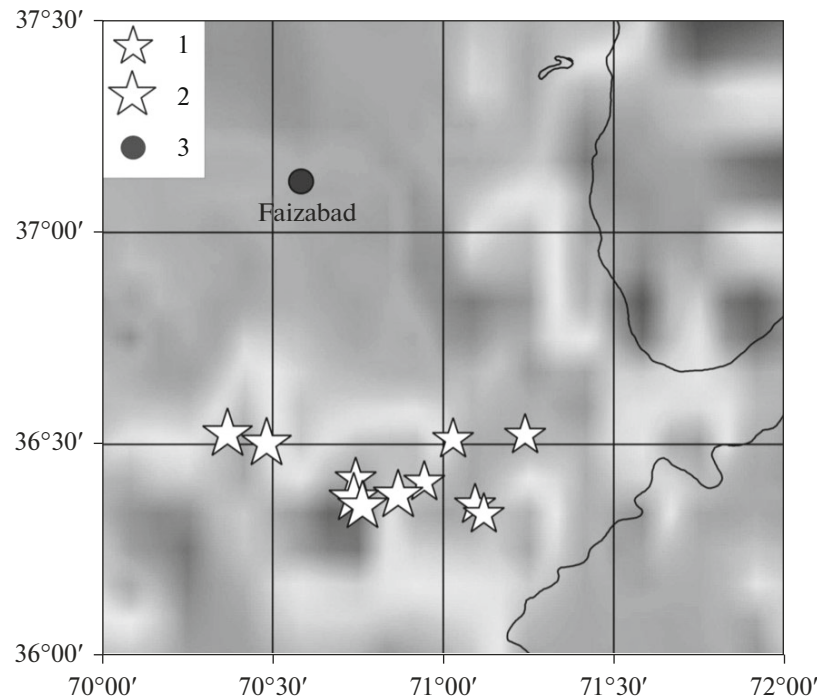


**Fig. 2.** The epicenters of large ( $M \geq 6.5$ ) earthquakes that occurred at depths of  $h > 100$  km since 1973. (1)  $M = 6.5-6.9$ ; (2)  $M \geq 7.0$ ; (3) large cities.

The role of the second factor was that when records at a station were for hypocenters at different depths the rays may pass different segments of their paths in an inhomogeneity of high attenuation. According to data obtained previously, the zones of the highest attenuation for S waves beneath central Tien Shan are generally in the lower crust, at depths of  $\sim 30-50$  km (Kopnichev and Sokolova, 2003; *Zemnaya kora ...*, 2006). The same depths also contain regions of the highest electrical conductivity as shown by MTS surveys (Bielinski et al., 2003). In both of these cases the effects are thought to result from the presence of an appreciable fraction of free fluids. In order to assess the second factor we considered ray displacements at the M interface from sources at different depths. For the sake of definiteness, we will use a simple two-layered earth model whose crust is  $h_c = 50$  km thick and whose shear velocities in the crust and upper mantle are 3.5 and 4.6 km/s, respectively. Table 2 lists ray shifts in the crust for sources at different depths. It follows from this table that for epicenters in the middle of the top layer and the bottom layer, the ray divergence at the M interface is  $\sim 3.5$  km. Now, the radius of the Fresnel zone  $R_f = \sqrt{(lk\lambda)}$  ( $lk$  is the length of the path segment that the ray passes within the crust and  $\lambda$  is the wavelength) is  $\sim 15$  km. Hence, we find that  $rk/R_f \ll 1$ , so that we can safely assume that any attenuation inhomogeneities in the lower crust would not produce significant differences in S/P for different source depths, all other things being equal.

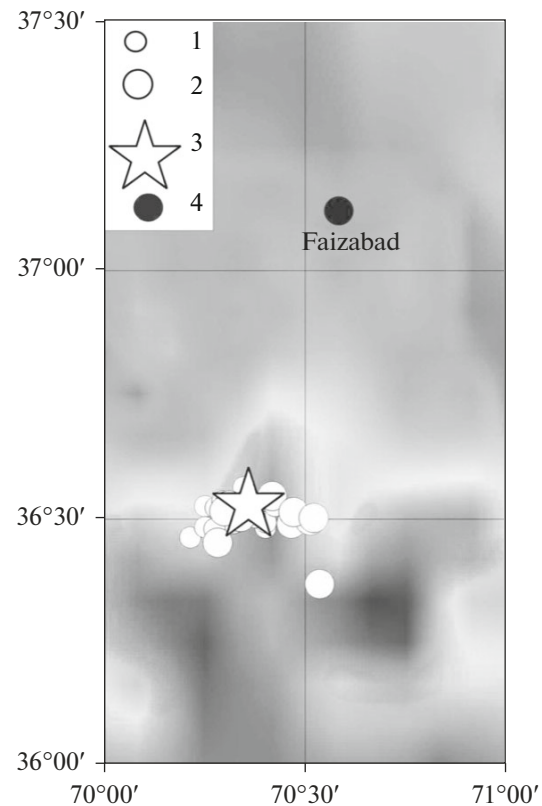


**Fig. 3.** The distribution of aftershocks of the October 26, 2015 earthquake (in map view). (1)  $M = 4.0-4.4$ ; (2)  $M \geq 4.5$ ; (3) the epicenter of the October 26, 2015 earthquake; (4) major cities.

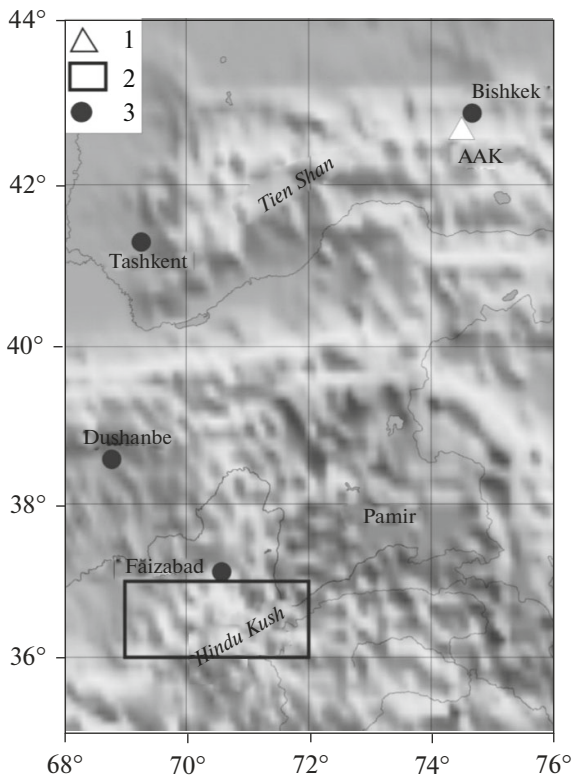


**Fig. 4.** The area of study. (1) seismic station; (2) source area; (3) major cities.

## DATA ANALYSIS

Figure 5 shows examples of typical records of earthquakes in the aftershock zone of the October 26, 2015 earthquake and its near environs in 2013–2015 (before that event). One can see that an event in the bottom layer produced a very low relative level of shear wave, while that in the second layer gave a high level. The records of events in the first and third layers are characterized by intermediate values of S/P.

**Table 2.** Estimating the ray offsets at the M interface for Hindu Kush earthquakes at different depths

$h$ , km	$ik^\circ$	$rk$ , km	$lk$ , km
170	48.3	56.1	75.0
200	47.7	54.9	74.3
220	47.3	54.2	73.7
250	46.5	52.6	72.6

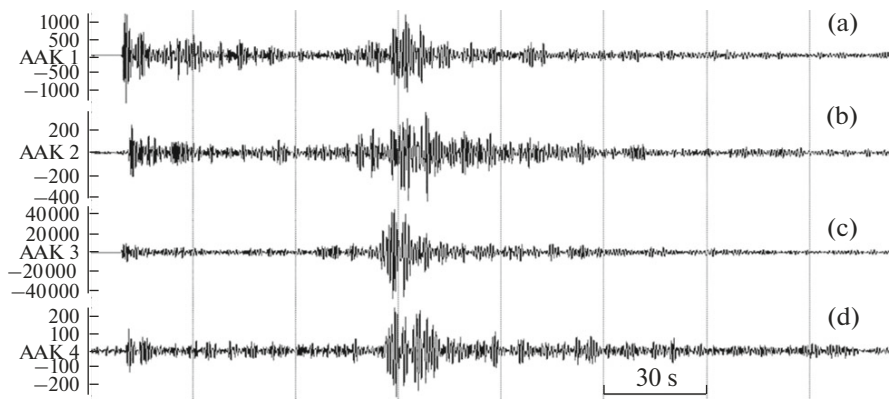
$ik$  denotes the angle that the ray makes with the vertical (in the crust),  $rk$  is the ray offset in the crust, and  $lk$  is the length of the crustal ray path.

For convenience, we will consider time-dependent variations in S/P starting from the bottom layer. Figure 6 shows S/P as a function of time for the layer (for brevity we denote it as S/P250; the index here and in what follows is the mean depth of the range). The confidence levels for mean values at 0.7 level vary between 0.04 and 0.18. One can see that the mean S/P250 values rapidly decrease over time for the western and central regions ( $69.80^\circ$ – $70.55^\circ$  E), from 0.48 in 1996–2000 to 0.02 in 2005–2014. At the same time, the variations in S/P250 for the eastern region (between  $70.55^\circ$  and  $71.30^\circ$  E) are much less pronounced (from 0.09 in 1994–1995 to 0.32 in 2015). We note that the average S/P250 for the 2015 events is outside the interval  $\pm\sigma$  based on the 1994–2014 data. At the same time, the value of S/P250 for the aftershocks of the October 26, 2015 earthquake rapidly increased and reached 0.64, thus falling outside the  $\pm 5\sigma$  interval.

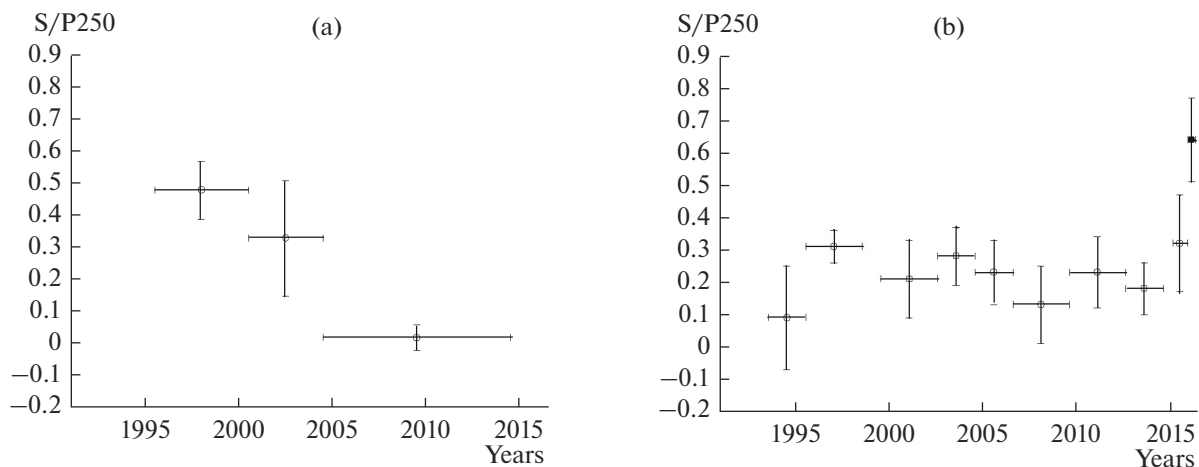
Figure 7 illustrates how S/P220 behaved as a function of time for the 211–230 km depth range. In the west, where all data are for the  $70.0^\circ$ – $70.2^\circ$  region, a relatively high level of mean values of that parameter was observed in 1995–2004 (occasionally reaching 0.56); S/P220 then decreased to 0.24 in 2013–2015. The S/P220 value varied comparatively slowly in the source region ( $70.20^\circ$ – $70.55^\circ$  E) during the 1994–2005 period (between 0.29 and 0.43) and then dropped to 0.20–0.29 in 2008–2012 and 2013–2015. It is important to mention that the S/P220 based on the aftershocks of the October 26, 2015 earthquake rapidly increased in the source region (reaching 0.66, which is outside the  $\pm 4\sigma$  interval). In the east, S/P220 is on the whole considerably below the values in the west and in the middle (variations between 0.03 and 0.29). Interestingly, the S/P220 parameter based on the aftershocks of the October 26, 2015 earthquake noticeably dropped (reaching 0.18), which is outside the  $\pm\sigma$  interval.

Figure 8 presents the S/P200 parameter plotted against time. In this case enough data were available only for the central and eastern regions. The central region showed a very high level of S/P200, which varied between 0.56 and 0.72 based on the data before October 26, 2015. We note that this parameter increased to reach 0.78 for the aftershocks of the large earthquake. For the eastern region the level of S/P200 was considerably lower; the overall variation was between 0.19 and 0.39, while dropping even as low as 0.06 for the aftershocks of the October 26, 2015 earthquake; this is outside the  $\pm 3\sigma$  interval.

Figure 9 shows the S/P170 parameter plotted against time (for the uppermost range of depth considered here). We have succeeded in estimating the mean value of the parameter only for the 2001–2013 period ( $S/P170 = 0.32 \pm 0.13$ ). For the central region (see Fig. 9a), the values of S/P170 are considerably higher, varying between 0.45 and 0.57. The most-abundant data were obtained for the eastern region. It follows



**Fig. 5.** Sample seismograms of deep-focus Hindu Kush earthquakes. AAK station, channel 1.25 Hz. (a) March 1, 2014,  $36.60^{\circ}$  N,  $70.49^{\circ}$  E,  $h = 250$  km; (b) May 11, 2015,  $36.49^{\circ}$  N,  $70.30^{\circ}$  E,  $h = 212$  km; (c) July 29, 2013,  $36.50^{\circ}$  N,  $70.54^{\circ}$  E,  $h = 207$  km; (d) August 10, 2015,  $36.50^{\circ}$  N,  $70.45^{\circ}$  E,  $h = 155$  km.



**Fig. 6.** Time-dependent variations in S/P250. (a) Western and central regions; (b) eastern region. Here and below, we show the means and confidence intervals at the 0.7 level. The horizontal bars mark the averaging intervals. The filled symbol is based on data for the aftershocks of the October 26, 2015 event.

from Fig. 9b that S/P170 was substantially lower there compared with the central region, varying between 0.20 and 0.42. It is of interest to note that in this case S/P remained within the interval  $\pm\sigma$  after the October 26, 2015 earthquake. We note that the event was not preceded by any considerable drop in S/P within the two upper layers in both of these regions, unlike the situation with the 211–230 and 231–270-km layers.

Figure 10 presents a scheme of the S-wave attenuation field in the area of study for the depth range 151–270 km that was largely based on the 2013–2015 data. However, two cases covered longer time spans (the western and central regions at depths of 231–270 km and the central region at depths of 151–190 km). The entire range of variation for the mean S/P parameter values was subdivided into three levels corresponding to a high (S/P = 0.00–0.10), an intermediate (S/P =

0.20–0.40), and a low (S/P = 0.45–0.70) shear-wave attenuation. It follows from Fig. 10 that prior to the October 26, 2015 earthquake the attenuation field in the zone of deep-focus seismicity was considerably inhomogeneous. The intermediate attenuation was observed in the eastern region throughout the entire range of considered depths, as well as in the western and central regions at depths of 211–270 km. At the same time, the 151–210 km depth range in the central region showed a substantially lower attenuation. High attenuation only occurred in the western and central regions at depths of 231–270 km. The greatest contrast in the parameter was observed in the central region between the second layer (S/P200 = 0.65) and the third layer (S/P220 = 0.29). From this we infer that the hypocenter of the large October 26, 2015 earthquake

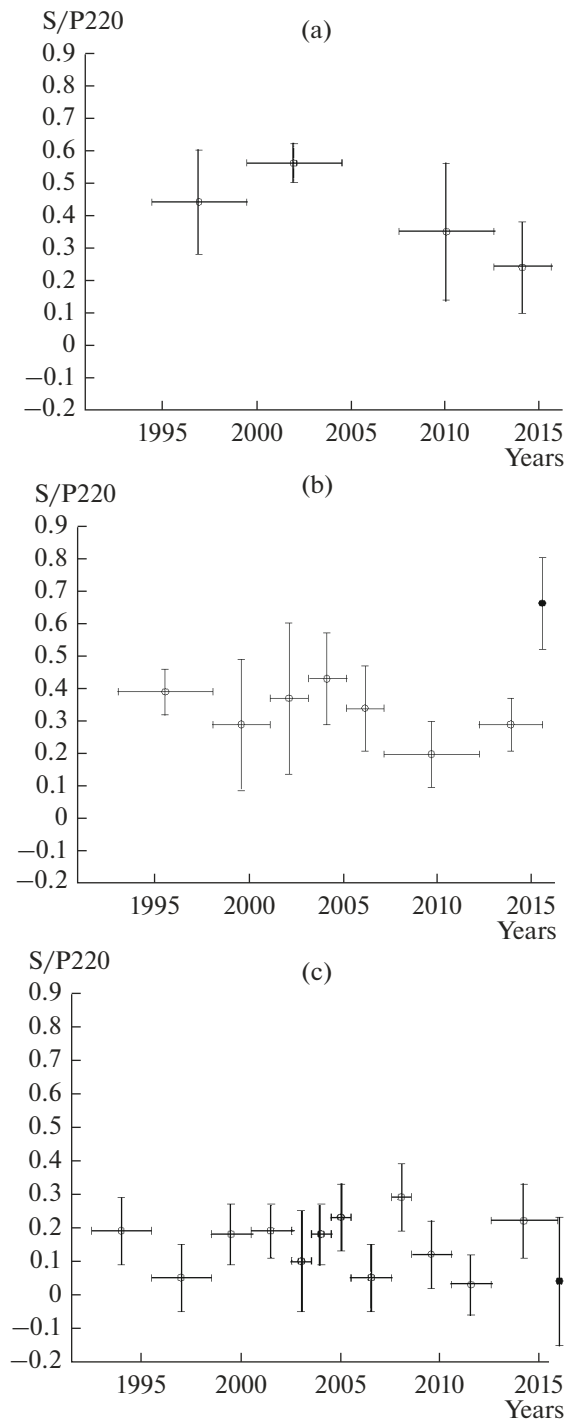


**Fig. 7.** Time-dependent variations in S/P220. (a) western region; (b) central region; (c) eastern region.

was in a volume of high attenuation, while most of its aftershocks occurred in a volume of lower attenuation.

Figure 11 shows a scheme of the attenuation field in the area of study based on the aftershocks of the October 26, 2015 earthquake that occurred between October 26, 2015 and March 31, 2016. It follows from this

figure that low attenuation was observed in the central region throughout the entire depth range. At the same time, the attenuation was intermediate in the eastern region in the top and bottom layers and higher in the two central layers. Comparison of Figs. 10 and 11 shows that the shear-wave attenuation was much lower in the central and eastern regions at depths of 211–270 and 231–270 km, respectively, following the October 26, 2015 earthquake, but increased in the eastern region at depths of 191–230 km.

These results show that the 2013–2015 mean S/P values were the lowest for the 231–270 km depth range and the highest for the 151–210 km range. At the same time, the time-dependent variations in S/P were much larger for the lower half of the section ( $h = 211–270$  km) than for the upper half.

## DISCUSSION

To summarize our results, substantial space–time variations in the S/P parameter were detected for Hindu Kush earthquakes in different ranges of depth. We note that these variations were little affected by the directivity of S and P wave radiation, since we averaged the data for each time interval. It can therefore be supposed that the most natural, and possibly the only, explanation of the effects detected here must relate to variations in the concentration of the liquid phase along the source–station paths. (It is known that a mere 1 vol % of the liquid phase would reduce the shear-wave velocity by 10% and lead to a drastic increase in attenuation (Hammond and Humpreys, 2000). We note that the time-dependent variations in the attenuation field observed here can only be caused by changes in the portion of fluids, not in that of partial melts, since melts have viscosities that are greater than fluid viscosity by many orders of magnitude. The changes in fluid concentration can occur both in the rupture zone (resulting from the migration of fluids, as well as from dehydration of mantle rocks, see Raleigh and Paterson, 1965; Kalinin et al., 1989; Yamasaki and Seno, 2003; Jung et al., 2004) and in the lower crust and uppermost mantle beneath recording stations (Kopnischev and Sokolova, 2007).

It was shown in (Kopnischev and Sokolova, 2003; *Zemnaya kora ...*, 2006) that the largest time-dependent variations in the attenuation field observed by the station in northern Tien Shan occurred in the lower crust. The above estimates indicate that the Fresnel zones largely overlap at the M interface beneath the observing station for different hypocenter depths. From this it follows that supposing that the variations in the S/P parameter resulted from changes in fluid concentration mostly in the lower crust beneath the station, they must have been nearly simultaneous for different regions in the source zone. At the same time, it follows from the above results that no correlation occurred between the S/P parameter values for different layers. In addition, there were several cases in

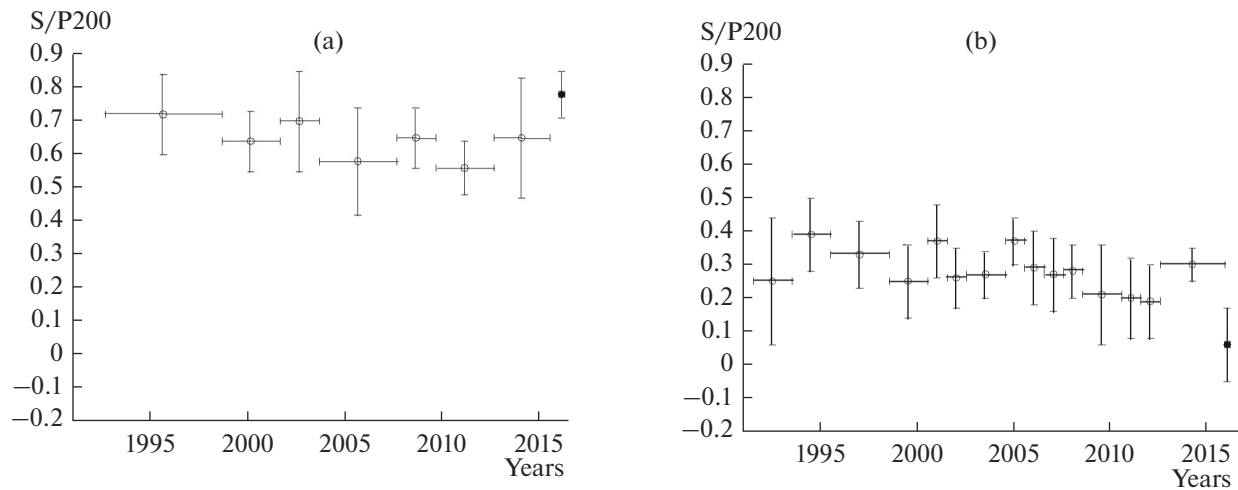


Fig. 8. Time-dependent variations in S/P200. (a) Central region; (b) eastern region.

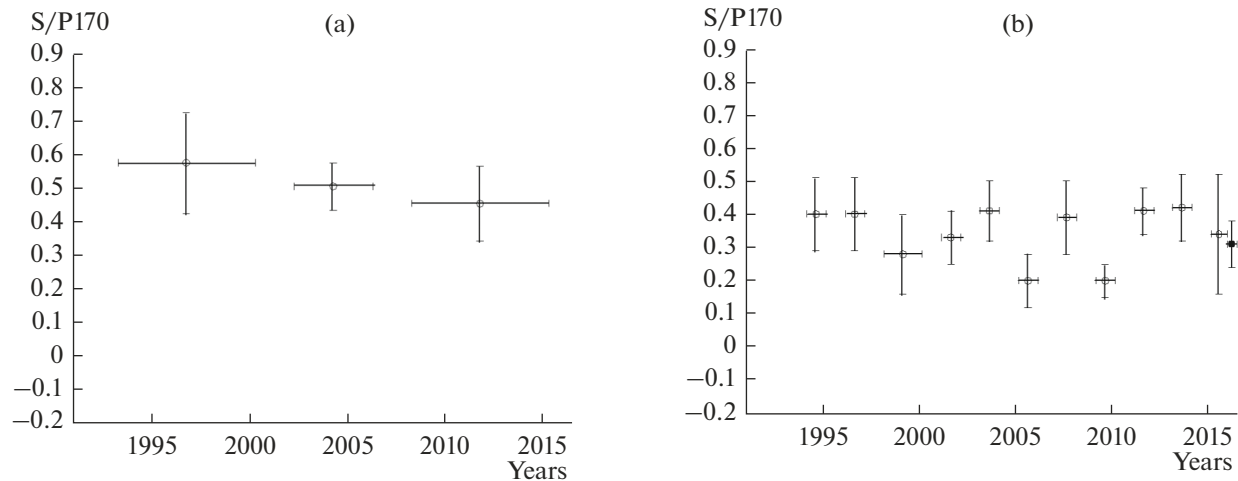


Fig. 9. Time-dependent variations in S/P170. (a) central region; (b) eastern region.

which the values experienced sharp changes at once after the October 26, 2015 earthquake, which occurred at an epicentral distance of  $\sim 770$  km from the AAK station. It thus appears that in the case considered here most of the variations in the S/P parameter were due to changes in fluid concentration in the deep-focus seismicity zone itself.

We note that the S/P variations can be divided into relatively slow and fast ones. Slow variations were observed for time spans between a few years and 10–20 years; they mostly involved gradual increases in attenuation. The greatest drop in S/P took place in the bottom layer, in the region between  $69.8^\circ$  and  $70.55^\circ$  E. At the same time, rapid variations (for a few months) were recorded for the aftershocks of the October 26, 2015 earthquake; they involved both increased attenuation (mostly in the eastern region at depths of 191–

230 km) and decreased one (in the central and eastern regions at depths of 211–270 and 231–270 km).

It may be hypothesized that the slow increases in attenuation (primarily in the two lower layers) were caused by dehydration of dense hydrosilicates that released free water (Raleigh and Paterson, 1965; Kalinin et al., 1989; Rodkin, 1993; Yamasaki and Seno, 2003; Jung et al., 2004). It is important to emphasize that dehydration is accompanied by embrittlement of crustal and mantle rocks, with these processes widely occurring in subduction zones (Yamasaki and Seno, 2003; Jung et al., 2004). It is natural to suggest that it was this effect that caused the large earthquake of October 26, 2015.

We also note that dehydration can gradually produce a connected network of pores and cracks filled with fluids. In that case there would be a stress con-

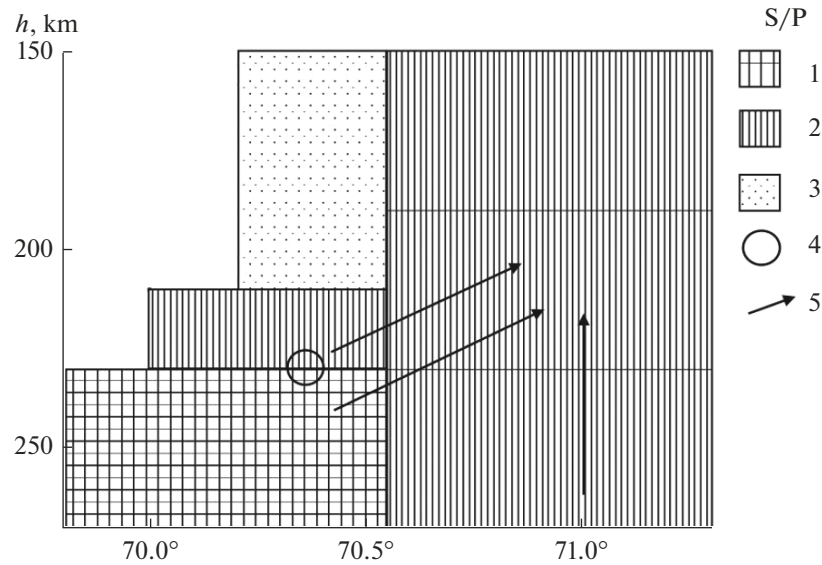


**Fig. 10.** A map of the attenuation field beneath Hindu Kush (data for January 1, 2013 through October 25, 2015). (1–3) attenuation (1, high; 2, intermediate; 3, low); (4) the hypocenter of the October 26, 2015; (5) inferred directions of fluid migration.

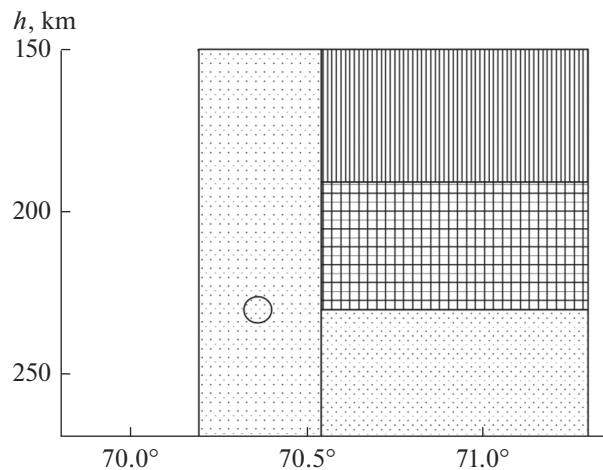


**Fig. 11.** A map of the attenuation field beneath Hindu Kush (data for October 26, 2015 through March 31, 2016). For the legend, see Fig. 10.

centration at the top of a two-phase layer where such a network exists (Karakin and Lobkovskii, 1982; Gold and Soter, 1984/1985), which can substantially contribute toward earthquake rupture.

At the same time, the rapid attenuation variations in the aftershocks of that earthquake were most likely due to “seismic pumping” (Sibson et al., 1975; Main et al., 2012), as well as to increased permeability resulting from vibration caused by a strong earthquake and a large number of aftershocks. The seismic pumping effect consists in fluids being injected into volumes of relative extension. In the cases under consideration here, such volumes tend to be due to the generation of large-amplitude seismic waves that travel outward from the rupture zone of a large earthquake. Such

occurrences are observed, in particular, at sufficiently large distances from the rupture zones of large earthquakes during the passage of low frequency surface waves (Miyazawa and Brodsky, 2008). Increased attenuation during long-continued vibration occurred even in modeling experiments (Barabanov et al., 1987) and is even more likely at relatively great depths in the upper mantle where the buoyant force tends to force lighter fluids upward.

These results show that after the October 26, 2015 earthquakes fluids most likely migrated from the bottom layer, as well as from the central region of the layer at depths of 211–230 km, into the second and third layers in the eastern region. This can explain synchronous oppositely directed variations in S/P in the



respective regions. The supply of an extra portion of fluids into the eastern region following the October 26, 2015 earthquake was most likely facilitated by the presence of an appreciable portion of the liquid fraction there before the event. Obviously, the passage of seismic waves makes it easier for fluids to migrate into fault zones or fractures that had previously been filled with the liquid phase. In this connection we note that the overwhelming majority of large earthquakes in the last 40 years occurred at depths of 190–230 km in the eastern region (see Fig. 2). It may be hypothesized that the relatively high attenuation that took place in the region before the October 26, 2015 event was due to the ascent of fluids after the nine large earthquakes that have been recorded in the region since 1973.

At the same time, fluids were obviously unable to penetrate from below into the central region of the second layer in considerable amounts. This may have been due to the fact that the region is dominated by hydrated rocks (which generally have lower viscosities, Kalinin et al., 1989). In this connection one important circumstance should be mentioned, viz., that a single large earthquake has occurred in the region during the 1973–2014 period, which does not seem to have added significantly to the available fluid portion at depths of 190–210 km. It was for this reason that the central region at these depths acted as a poorly permeable barrier that did not allow fluids to rise still higher.

At the same time, it can be supposed that the large earthquake of October 26, 2015 initiated dehydration of mantle rocks in this region and thus made them more brittle; this would explain the extremely numerous aftershocks in the rupture zone at depths of 190–210 km. We know that dehydration requires extra energy (Kalinin et al., 1989); this energy can be supplied by the energy of high-amplitude seismic waves.

There is thus strong reason to believe that great deep-focus earthquakes in the Hindu Kush area occurred because of dehydration and the ascent of deep-seated fluids into earthquake source zones. It should be noted that dehydration of oceanic crust and the ascent of fluids have long been known to occur at subduction zones; however, they are observed at these features at considerably shallower depths (commonly not deeper than 70 km, Yamasaki and Seno, 2003). The great depths at which these processes are observed beneath Hindu Kush are obviously due to much lower heating of the upper mantle there; this is supported, in particular, by the absence of young volcanism, as well as by very high seismic velocities at depths of approximately 200 km (Roecker, 1982).

We conclude by noting that dehydration, as well as the ascent of deep-seated fluids, constitute a reflection of self-organization processes in geological systems (Letnikov, 1992); this ultimately reduces the Earth's potential energy.

## REFERENCES

- Barabanov, V.L., Grinevskii, A.O., Kissin, I.G., and Nikolaev, A.V., On some effects of vibrational seismic excitation on a water-saturated medium. Comparing these to effects of large remote earthquakes, *Dokl. Akad. Nauk SSSR*, 1987, vol. 297, no. 1, pp. 53–56.
- Bielinski, R., Park, S., Rybin, A., et al., Lithospheric heterogeneity in the Kyrgyz Tien Shan imaged by magnetotelluric studies, *Geophys. Res. Lett.*, 2003, vol. 30, no. 15. doi 10.1029/2003GL017455
- Hammond, W. and Humpreys, E., Upper mantle seismic wave velocity: effects of realistic partial melt geometries, *J. Geophys. Res.*, 2000, vol. 105, pp. 10 975–10 986.
- Gold, T. and Soter, S., Fluid ascent through the solid lithosphere and its relation to earthquakes, *Pageoph.*, 1984/1985, vol. 122, pp. 492–530.
- Jung, H., Green, H., and Dobrzhinetskaya, L., Intermediate-depth earthquake faulting by dehydration embrittlement with negative volume change, *Nature*, 2004, vol. 428, pp. 545–549.
- Kalinin, V.A., Rodkin, M.V., and Tomashevskaya, I.S., *Geodinamicheskie efekty fiziko-khimicheskikh prevrashchenii v tverdoi srede* (Geodynamic Effects Due to Physical and Chemical Transformations in Solids), Moscow: Nauka, 1989.
- Karakin, A.V. and Lobkovskii, L.I., Hydrodynamics and structure of a two-phase asthenosphere, *Dokl. Akad. Nauk SSSR*, 1982, vol. 268, no. 2, pp. 324–329.
- Kopnichev, Yu.F., *Korotkoperiodnye seismicheskie volnovye polya* (Short Period Seismic Wave Fields), Moscow: Nauka, 1985.
- Kopnichev, Yu.F., Baskutas, I., and Sokolova, I.N., Double large earthquakes and geodynamic processes in Central and South Asia, *Vulkanol. Seismol.*, 2002, no. 5, pp. 49–58.
- Kopnichev, Yu.F. and Sokolova, I.N., Space–time variations of the S wave attenuation field in the rupture zones of large Tien Shan earthquakes, *Fizika Zemli*, 2003, no. 7, pp. 35–47.
- Kopnichev, Yu.F. and Sokolova, I.N., Heterogeneities in the field of short period seismic wave attenuation in the lithosphere of Central Tien Shan, *J. Volcanol. Seismol.*, 2007, vol. 1, no. 5, pp. 333–348.
- Letnikov, F.A., *Sinergetika geologicheskikh sistem* (The Synergetics of Geological Systems), Novosibirsk: Nauka, 1992.
- Levin, B.V. and Sasorova, E.V., *Seismichnost' Tikhookeanskogo regiona. Vyyavlenie global'nykh zakonomernostei* (Seismicity of the Pacific Region. Identification of Global Patterns), Moscow: Yanus-L, 2012.
- Main, I., Bell, A., Meredith, P., et al., The dilatancy–diffusion hypothesis and earthquake predictability, *J. Geol. Soc.*, 2012, vol. 367, pp. 215–230.
- Miyazawa, M. and Brodsky, E., Deep low-frequency tremor that correlates with passing surface waves, *J. Geophys. Res.*, 2008, vol. 113, no. B01307. doi 10.1029/2006JB004890
- Ogawa, R. and Heki, K., Slow postseismic recovery of geoid depression formed by Sumatra–Andaman earth-

- quake by mantle water diffusion, *Geophys. Res. Lett.*, 2007, vol. 34. L06313. doi 10.1029/2007GL029340
- Pegler, G. and Das, S., An enhanced image of the Pamir-Hindu Kush seismic zone from relocated earthquake hypocenters, *Geophys. J. Int.*, 1998, vol. 134, pp. 573–595.
- Raleigh, C. and Paterson, M., Experimental deformation of serpentine and its tectonic implications, *J. Geophys. Res.*, 1965, vol. 70, pp. 3965–3985.
- Rodkin, M.V., *Rol' glubinnogo flyuidnogo rezhima v geodinamike i seismotektonike* (The Role of Fluid Behavior at Depth in Geodynamics and Seismotectonics), Moscow, 1993.
- Roecker, S., Velocity structure of the Pamir-Hindu Kush region: possible evidence of subducted crust, *J. Geophys. Res.*, 1982, vol. 87, pp. 945–959.
- Roecker, S., Soboleva V., Nersesov, I., et al., Seismicity and fault plane solutions of intermediate depth earthquakes in Pamir-Hindu Kush region, *J. Geophys. Res.*, 1980, vol. 85, pp. 1358–1364.
- Sibson, R., Moore, J., and Rankin, A., Seismic pumping—a hydrothermal fluid transport mechanism, *J. Geol. Soc.*, 1975, vol. 131, pp. 653–659.
- Yamasaki T. and Seno, T., Double seismic zone and dehydration embrittlement of the subducting slab, *J. Geophys. Res.*, 2003, vol. 108, no. B4. doi 0.1029/2002JB001918
- Zemnaya kora i verkhnyaya mantiya Tyan'-Shanya v svyazi s geodinamikoi i seismichnost'yu* (The Crust and Upper Mantle beneath Tien Shan in Connection with Geodynamics and Seismicity), Bakirov, A.B., Ed., Bishkek: Ilim, 2006.

*Translated by A. Petrosyan*